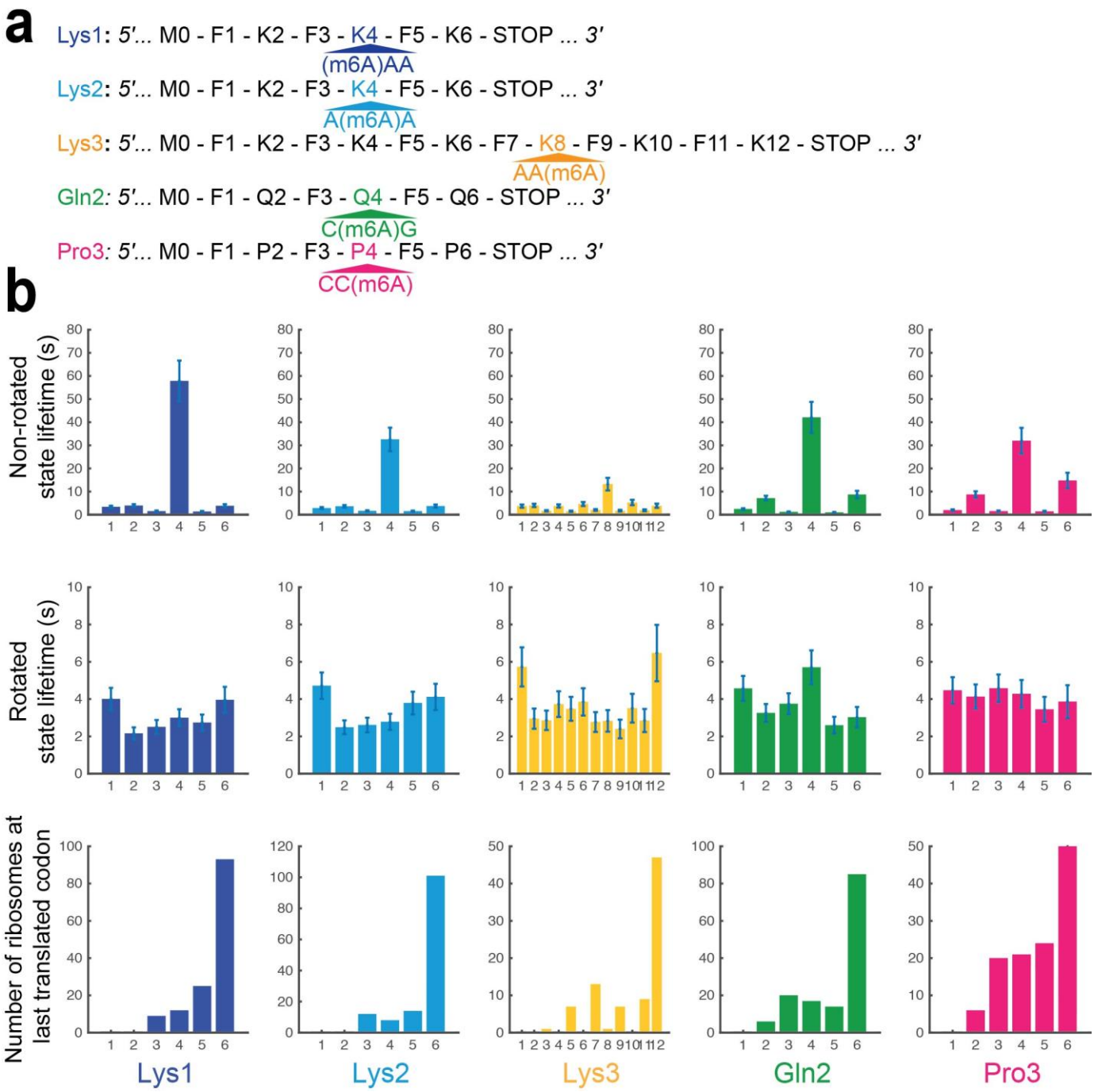

Supplementary Figure 1

Comparing rotated- and nonrotated-state lifetimes among mRNA m^6A modifications in different codon contexts.

a. mRNA sequences used for each experiments, as same as shown in **Figure 2a**.
b. The rotated state and non-rotated state lifetime measurements for all codons in the mRNAs used. First row shows the non-rotated state lifetimes for each codons within the mRNAs, and second row shows the rotated state lifetimes for each codons within the mRNAs. Last row shows the number of ribosomes observed to reach particular codon during translation prior to photobleaching of reporter fluorescence dye.

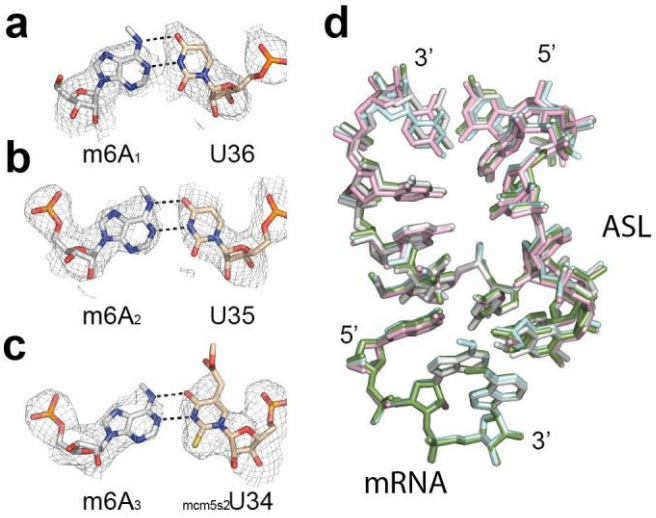

Supplementary Figure 2

Geometry of the m^6A-uridine Watson-Crick base-pair interactions.

The final σ_A-weighted $m2F_o$-dF_c electron density map contoured at 1σ level shows that **a.** $m6A_1$•U36, **b.** m6A•U35 and **c.** m6A•$_{mcm5s2}$U34 base pairs are in the Watson-Crick geometry. ASL carbons are colored wheat and mRNA carbons are gray. **d.** The overlay of all structures reveals a nearly identical orientation of the codon:anticodon interaction). The ASL^{Lys3}_{UUU}–AAA complex (colored in gray), the ASL^{Lys3}_{UUU} – (m6A)AA (colored in light pink), ASL^{Lys3}_{UUU} –A(m6A)A (colored in cyan) and ASL^{Lys3}_{UUU} –AA(m6A) (colored in green) are superposed and aligned with respect to the 16S rRNA.

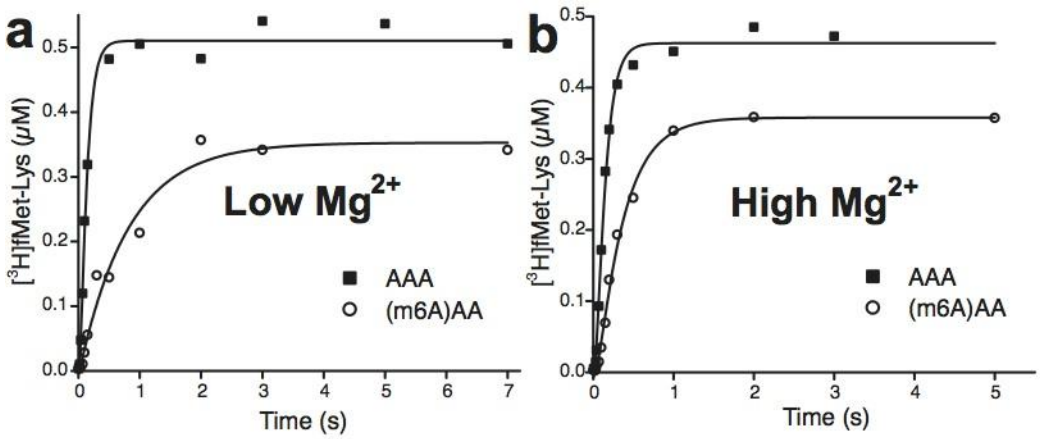

Supplementary Figure 3

Proofreading of $tRNA^{Lys}$ ternary complexes reading (m^6A)AA.

Dipeptide formation was measured at 1μM ribosomes and 0.5 μM ternary complexes. Experiments were done in parallel using the very same ternary complexes reacting with initiation complexes displaying AAA or (m6A)AA codon in the A site. The lower plateau of dipeptide fMet-Lys formation for (m6A)AA indicates the rejection of $tRNA^{Lys}$ after GTP hydrolysis.
a. Experiments were done in low Mg^{2+} buffer (see Methods). Proofreading factor, f = 1.5, was calculated as the ratio between the plateaus of dipeptide formation for AAA and (m6A)AA.
b. Same experiment was performed in high Mg^{2+} buffer (see Methods), where proofreading factor was measured to be f = 1.3.

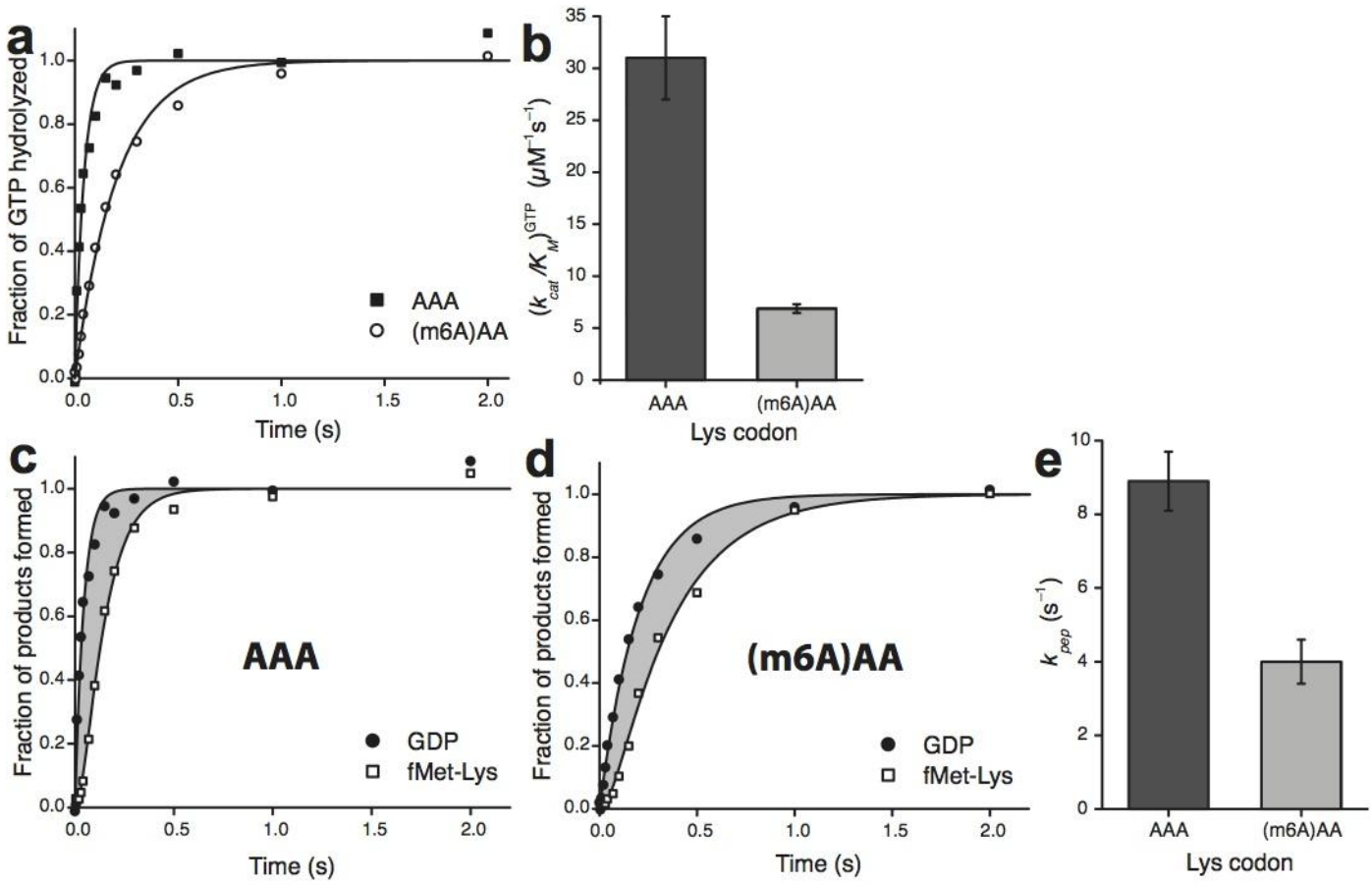

Supplementary Figure 4

Reducing decoding accuracy reduces the effect of m^6A on translational dynamics in high-Mg^{2+} conditions.

(**a**) Kinetics of GTP hydrolysis after binding of Lys-$tRNA^{Lys}$ ternary complexes (0.2 μM) to 70S initiation complexes (0.7μM) programmed with AAA or (m6A)AA in the A site. (**b**) Estimates of k_{cat}/K_M-values for GTP hydrolysis. (**c**) and (**d**) Kinetics of GTP hydrolysis and dipeptide fMet-Lys formation measured simultaneously in the very same experiment. The grey areas represent the total time for all subsequent steps after GTP hydrolysis up to and including peptidyl transfer. (**e)** Estimates of the compounded rate constant, k_{pep}, for the steps after GTP hydrolysis on EF-Tu up to and including peptidyl transfer, from experiments shown in **c** and **d**. See **Supplementary Data Table 1** for data in **b** and **e**. Kinetic data in **a**, **c**, and **d** are representative of three independent experiments. Error bars in **b** and **e** represent SD (n = 3, technical replicates) as calculated from the fitting procedure **(**Johansson, M. *et al. Proc. Natl. Acad. Sci. U. S. A.* **108,** 79–84 (2011)).

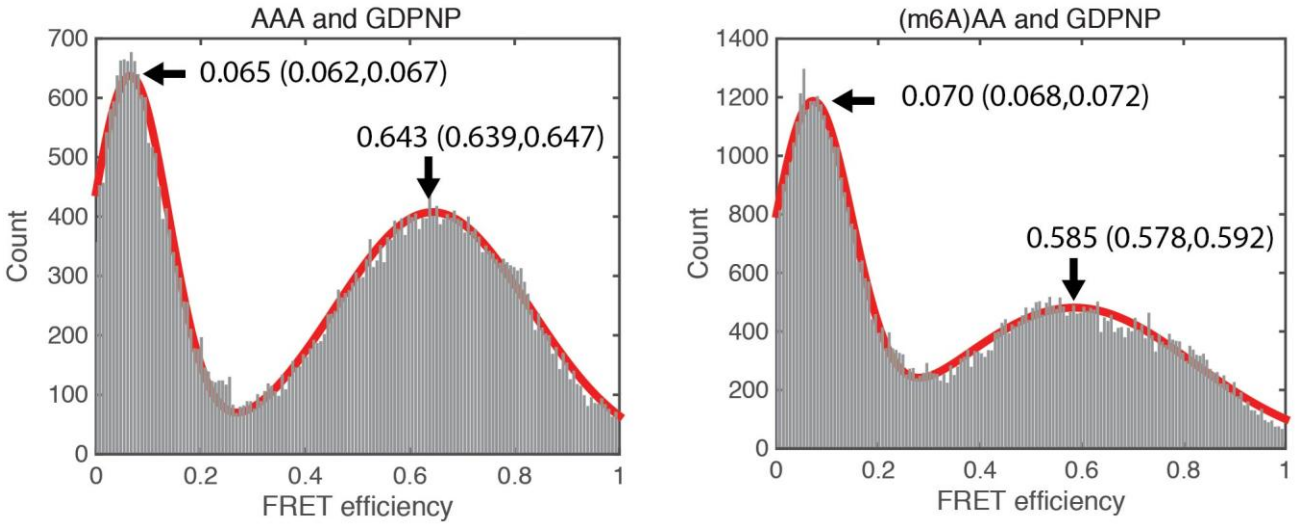

Supplementary Figure 5

m^6A shifts FRET value between P-site tRNA and A-site tRNA in the GTPase-activated state.

FRET histogram of the GDPNP-induced prolonged GTPase-activated state and codon-recognition states for unmodified (left) and first-base m6A modified (right) cases at 15mM magnesium concentration. Values inserted indicate fitted center of Gaussian distribution to histogram, and values in parenthesis indicate 95% confidence interval of fitting. While peaks near 0 FRET efficiency indicates no FRET state, peaks near 0.6 FRET efficiency corresponds to GTPase-activated state. FRET efficiency decreases slightly from 0.643 to 0.585 when cognate AAA codon is modified to (m6A)AA codon, mirroring previous comparison between cognate and near-cognate pairing on Phe (Lee, T., Blanchard, S. C., Kim, H. D., Puglisi, J. D. & Chu, S. The role of fluctuations in tRNA selection by the ribosome. *Proc. Natl. Acad. Sci.* **104,** 13661–13665 (2007)).

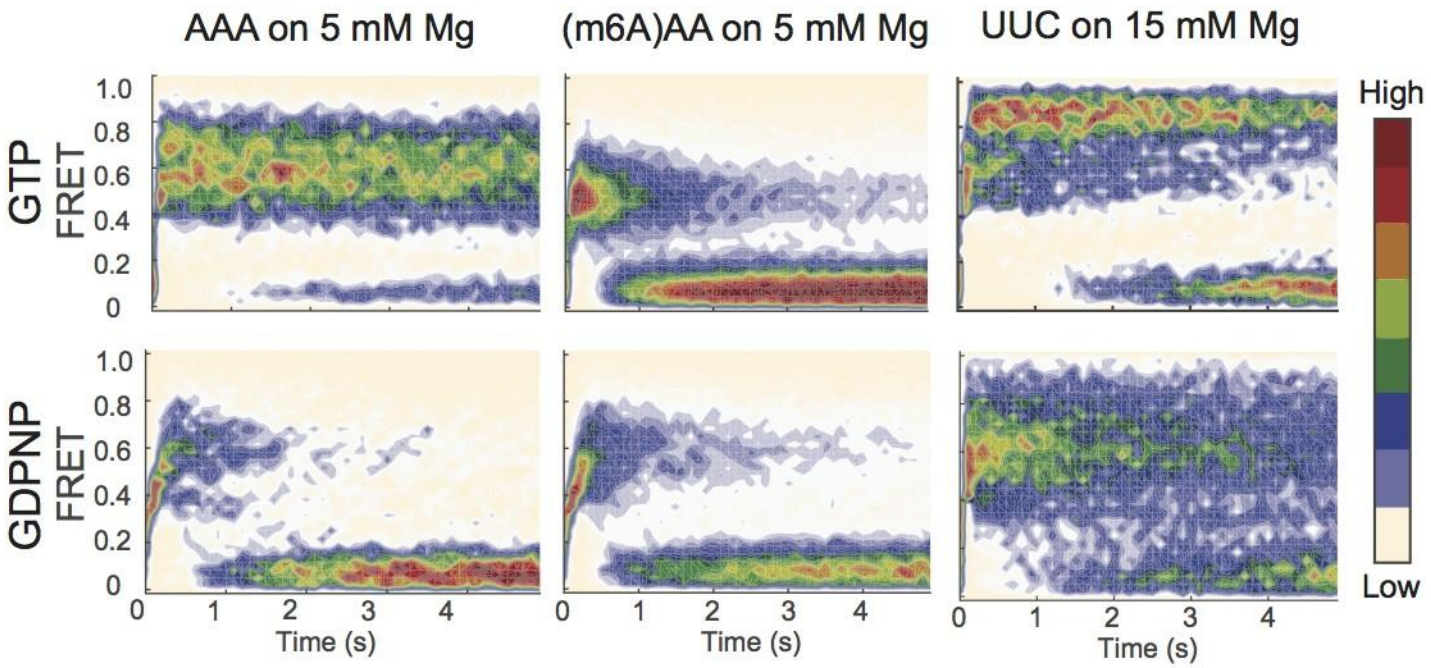

Supplementary Figure 6

tRNA-tRNA FRET lifetime decreases severely with m^6A at low magnesium.

Comparing representative synchronized FRET time evolution between different conditions. Low magnesium condition aggravates the effect of m6A in tRNA recognition by increasing accuracy of tRNA selection of ribosome (top left, top middle panel), which inverts ratio between successful accommodation event and transient sampling event compared to high magnesium condition. When decoding is further hindered by GDPNP at low magnesium condition, FRET lifetime at GTPase-activated state decreases and the effect of m6A cannot be detected accurate in our current time resolution of 100 millisecond; decreased FRET event lifetime due to m6A might be less than 100 millisecond, which our measurement would only sample long-lived FRET events rather than giving a correct lifetime. We also performed tRNA FRET between P site fMet-(Cy3)$tRNA^{fMet}$ and A site Phe-(Cy5)$tRNA^{Phe}$ binding to UUC codon at A site, similar to previously published result for comparison (rightmost two panels). Number of FRET events post-synchronized for each experiment is 316, 213, 497, 577, 221, and 781 for GTP-AAA, GTP-(m6A)AA, GDPNP-AAA, GDPNP-(m6A)AA, GTP-UUC and GDPNP-UUC, respectively.

Supplementary Table 1 Kinetic parameters for $tRNA^{Lys}$ ternary complex reading codon AAA and (m6A)AA.

Buffer [1]	Lys codon	$(k_{cat}/K_M)^{GTP}$ ($\mu M^{-1}s^{-1}$) [2]	Proofreading factor (f) [3]	k_{pep} (s^{-1}) [4]
Low Mg^{2+}	AAA	14.6 ± 0.8	1.0	12.2 ± 0.7
	(m6A)AA	1.25 ± 0.07	1.5	7.2 ± 1.4
High Mg^{2+}	AAA	31 ± 4	1.0	8.9 ± 0.8
	(m6A)AA	6.9 ± 0.4	1.3	4.0 ± 0.6

[1] Low Mg^{2+} buffer contained 1.3 mM free Mg^{2+}; high Mg^{2+} buffer contained 7.5 mM free Mg^{2+}. See Methods.

[2] k_{cat}/K_M values for GTP hydrolysis. Related to **Figure 3c** for low Mg^{2+} buffer and **Supplementary Figure 4b** for high Mg^{2+} buffer.

[3] Related to **Supplementary Figure 3**.

[4] Compounded rate constant for the steps after GTP hydrolysis on EF-Tu up to and including peptidyl transfer. Related to **Figure 3f** for low Mg^{2+} buffer and **Supplementary Figure 4e** for high Mg^{2+} buffer.